

On the fundamental dichotomy in the local radio-AGN population: accretion, evolution, and host galaxy properties

P. N. Best,^{1*} and T. M. Heckman²

¹ SUPA†, Institute for Astronomy, Royal Observatory Edinburgh, Blackford Hill, Edinburgh EH9 3HJ

² Department of Physics & Astronomy, The Johns Hopkins University, Baltimore, MD 21218, USA

27 November 2024

ABSTRACT

A sample of 18286 radio-loud AGN is presented, constructed by combining the 7th data release of the Sloan Digital Sky Survey with the NRAO VLA Sky Survey (NVSS) and the Faint Images of the Radio Sky at Twenty centimetres (FIRST) survey. Using this sample, the differences between ‘high-excitation’ (or ‘quasar-mode’; hereafter HERG) and ‘low-excitation’ (‘radio-mode’; LERG) radio galaxies are investigated. A primary difference between the two radio source classes is the distinct nature of the Eddington-scaled accretion rate onto their central black holes: HERGs typically have accretion rates between one per cent and ten per cent of their Eddington rate, whereas LERGs predominately accrete at a rate below one per cent Eddington. This is consistent with models whereby the population dichotomy is caused by a switch between radiatively efficient and radiatively inefficient accretion modes at low accretion rates. Local radio luminosity functions are derived separately for the two populations, for the first time, showing that although LERGs dominate at low radio luminosity and HERGs begin to take over at $L_{1.4\text{GHz}} \sim 10^{26} \text{W Hz}^{-1}$, examples of both classes are found at all radio luminosities. Using the V/V_{max} test it is shown that the two populations show differential cosmic evolution at fixed radio luminosity: HERGs evolve strongly at all radio luminosities, while LERGs show weak or no evolution. This suggests that the luminosity-dependence of the evolution previously seen in the radio luminosity function is driven, at least in part, by the changing relative contributions of these two populations with luminosity. The host galaxies of the radio sources are also distinct: HERGs are typically of lower stellar mass, with lower black hole masses, bluer colours, lower concentration indices, and less pronounced 4000\AA breaks indicating younger stellar populations. Even if samples are matched in radio luminosity and stellar and black hole masses, significant differences still remain between the accretion rates, stellar populations, and structural properties of the host galaxies of the two radio source classes. These results offer strong support to the developing picture of radio-loud AGN in which HERGs are fuelled at high rates through radiatively-efficient standard accretion disks by cold gas, perhaps brought in through mergers and interactions, while LERGs are fuelled via radiatively inefficient flows at low accretion rates. In this picture, the gas supplying the LERGs is frequently associated with the hot X-ray haloes surrounding massive galaxies, groups and clusters, as part of a radio-AGN feedback loop.

Key words: galaxies: active — radio continuum: galaxies — galaxies: jets — black hole physics — accretion, accretion discs

1 INTRODUCTION

Active Galactic Nuclei (AGN) are associated with the accretion of material onto supermassive black holes, of roughly a million to a billion solar masses, located near the centres of their host galaxies. Supermassive black holes are found in essentially all massive galaxies (e.g. Magorrian et al. 1998),

* Email: pnb@roe.ac.uk

† Scottish Universities Physics Alliance

with a mass that correlates strongly with the stellar mass (e.g. Marconi & Hunt 2003; Häring & Rix 2004) or velocity dispersion (e.g. Gebhardt et al. 2000; Ferrarese & Merritt 2000) of the surrounding galaxy bulge. It is now widely accepted that the build-up of these supermassive black holes and that of their host spheroids are intimately linked. Evidence is growing that AGN activity may play an important role in the evolution of the host galaxy, with AGN outflows being responsible for controlling or terminating star-formation (e.g. see review by Cattaneo et al. 2009).

AGN activity occurs in at least two different modes, each of which may have an associated, yet different, feedback effect upon the host galaxy. The most commonly-considered mode of AGN activity is the ‘standard’ accretion mode associated with quasars. In this mode, which has been variously referred to as ‘quasar-mode’, ‘cold-mode’, ‘radiative mode’, ‘fast-accretor’, ‘high-excitation’, or ‘strong-lined’, material is accreted onto the black hole through a radiatively-efficient, optically-thick, geometrically thin accretion disk (e.g. Shakura & Sunyaev 1973). These AGN radiate across a very broad range of the electromagnetic spectrum (e.g. Elvis et al. 1994) although a dusty structure surrounding the black hole and accretion disk, often referred to as a torus, obscures the emission at some wavelengths when the AGN is seen edge-on (Antonucci 1993, and references therein). They are often associated with star-formation activity in the host galaxies (e.g. Kauffmann et al. 2003a), although possibly with delays between the star formation and the AGN activity (e.g. Wild et al. 2010; Tadhunter et al. 2011, and references therein). A fraction of these AGN are radio-loud, possessing powerful radio jets that can extend for tens or hundreds of kpc.

This radiatively-efficient accretion mode may be important in curtailing star formation at high redshifts and setting up the tight relationship between black hole and bulge masses observed in the nearby Universe (e.g. Silk & Rees 1998; Fabian 1999; King 2003; Robertson et al. 2006). Observational evidence that quasars can accelerate high-velocity winds is plentiful, although there is much debate as to whether these are thermal ‘energy-driven’ winds, or ‘momentum-driven’ by radiation pressure (e.g. Cattaneo et al. 2009, and references therein). In radio-loud AGN, the powerful radio jets may also shock-accelerate the gas (e.g. Best et al. 2000), driving bipolar winds at speeds up to thousands of km/s (e.g. Nesvadba et al. 2008). Considerable uncertainty remains as to the mass and energy content of material that is driven out by these winds, the size-scale of the outflows in radio-quiet quasars, and the relative importance of the different mechanisms that may drive the winds.

There is a second mode of AGN activity, in which the accretion of material on to the black hole leads to little radiated energy, but can lead to the production of highly-energetic radio jets. It was first noted by Hine & Longair (1979) that a population of low luminosity radio sources exist in which the strong emission lines normally found in powerful AGN were absent. It has since been shown that these radio sources also exhibit no accretion-related X-ray emission, nor infrared emission from a putative torus (e.g. Hardcastle et al. 2007, and references therein), and are thus intrinsically different from the quasar-like AGN. Best et al. (2005a) showed that these low-luminosity radio sources are

hosted by fundamentally different host galaxies to emission-line selected (quasar-like) AGN, in terms of their stellar masses and host galaxy properties. These AGN, which have been referred to as ‘radiatively inefficient’, ‘radio-mode’, ‘hot-mode’, ‘slow-accretor’, ‘low-excitation’, or ‘weak-lined’, are believed to be fuelled through advection-dominated accretion flows (ADAFs), which are optically thin, geometrically thick, accretion flows (e.g. Narayan & Yi 1995). They emit the bulk of their energy in kinetic form through the radio jets (e.g. Merloni & Heinz 2007); debate remains as to whether all of the energy of the jets is associated with accretion, or whether energy from the spin of the supermassive black hole is also tapped (McNamara et al. 2011, and references therein).

Although the total cosmic contribution of the energetic output of jets is nearly two orders of magnitudes lower than that of radiation from the ‘quasar-mode’ AGN (e.g. Cattaneo & Best 2009), the jet energy is all deposited locally to the system, potentially producing a very efficient feedback mechanism. This is most directly observed in the bubbles and cavities that radio-AGN are observed to evacuate in the hot hydrostatic gas haloes of their host galaxies or surrounding groups and clusters (e.g. Böhringer et al. 1993; Carilli et al. 1994; McNamara et al. 2000; Fabian et al. 2006). The energies estimated for the radio sources correlate well with the Bondi accretion rates expected from the hot gas (Allen et al. 2006); this suggests that this hot gas may form both the fuel for the radio source, and the repository of its energy, offering the potential for a feedback cycle.

‘Radio-mode’ AGN have been widely used in galaxy formation models as a mechanism to switch off star formation in the most massive galaxies, thus reproducing both the observed shape of the galaxy luminosity function and the “old, red and dead” nature of massive early-type galaxies (Croton et al. 2006; Bower et al. 2006). Best et al. (2005b) showed that the prevalence of radio-AGN activity was a very strong function of the mass of the host galaxy, rising to over 30% in the most massive systems. Using a scaling relation between the radio luminosity and the mechanical energy of the jet (cf. Birzan et al. 2004; Cavagnolo et al. 2010), Best et al. (2006) went on to show that the time-averaged energetic output of these sources is indeed sufficient to counter-balance gas cooling in early-type galaxies of all masses. On a larger-scale, radio-AGN are almost ubiquitous in the brightest cluster galaxies of cool-core clusters (Burns 1990; Best et al. 2007), and have been invoked as the solution to both the ‘cooling flow’ and the ‘entropy floor’ problems in the intra-cluster medium of groups and clusters (McNamara & Nulsen 2007, and references therein).

The radiatively inefficient and radiatively efficient AGN clearly have fundamental differences, but the precise origin of these differences remains unclear. Some authors have argued that it relates to the origin of the fuelling gas, with accretion of cold gas leading to a stable accretion disk and a radiatively efficient accretion, while the accretion of hot gas via the Bondi mechanism would produce the jet-dominated radiatively inefficient AGN (e.g. Hardcastle et al. 2007). Others argue that the spin of the black hole is important (McNamara et al. 2011; Martínez-Sansigre & Rawlings 2011). A third hypothesis is that it is solely (or primarily) driven by the Eddington-scaled accretion rate onto the black

hole, with the ADAF mode occurring when the accretion rate is well below the Eddington limit. This was the prediction in the original work of Narayan & Yi (1995), and support for this picture has come from recent work indicating that broad-line AGN (ie. quasar-like AGN seen face-on) have lower limits to their accretion rates at around 1 percent of Eddington (Kollmeier et al. 2006; Trump et al. 2009a, 2011), and indications that a switch between flat-spectrum radio quasars and BL Lac objects (which are believed to be beamed versions of the radiatively-inefficient sources) also occurs at that Eddington rate (Wu et al. 2011; Ghisellini et al. 2011). This hypothesis is used by synthesis models for AGN evolution (e.g. Merloni & Heinz 2008) that have been constructed based upon the two different accretion modes.

A critical input to these AGN evolution models, and to understanding the evolving feedback role that AGN may play in galaxy evolution (cf. Croton et al. 2006; Bower et al. 2006) is a full understanding of the different AGN populations, their distribution in luminosity, their host galaxies, and their cosmic evolution. The cleanest method for selecting samples of radiatively inefficient AGN is through radio selection, using the emission of their jets. Radiatively inefficient AGN are detectable at other wavelengths: in particular, around 30% of the population of ‘X-ray bright optically normal’ galaxies found in X-ray surveys show X-ray spectra with no absorption, yet no evidence of AGN activity at optical wavelengths (Trump et al. 2009b), and are interpreted as being radiatively inefficient AGN in which the X-rays relate to a beamed component of the jet emission (Hart et al. 2009). Nevertheless, only at radio wavelengths is the selection function well-understood, and large samples can be constructed. In addition, corresponding samples of radiatively efficient (radio-loud) AGN can be constructed at the same time in exactly the same manner, allowing direct comparisons between the two.

This paper presents a large sample of radio sources drawn from the Sloan Digital Sky Survey (SDSS; York et al. 2000), and compares the properties of radio-selected radiatively efficient and inefficient AGN. The selection of the sample and the classification of the radio sources is described in Section 2. Section 3 investigates the nature of the radio sources: their accretion rates, their luminosity function, and their cosmic evolution. Section 4 compares various properties of the host galaxies of the two classes of sources. The results are discussed and conclusions drawn in Section 5. Throughout the paper, the cosmological parameters are assumed to have values of $\Omega_m = 0.3$, $\Omega_\Lambda = 0.7$, and $H_0 = 70 \text{ km s}^{-1} \text{ Mpc}^{-1}$.

2 SAMPLE SELECTION AND PROPERTIES

2.1 The overall radio source sample

The sample of radio sources was constructed by combining the 7th data release (DR7; Abazajian et al. 2009) of the SDSS spectroscopic sample with the National Radio Astronomy Observatory (NRAO) Very Large Array (VLA) Sky Survey (NVSS; Condon et al. 1998) and the Faint Images of the Radio Sky at Twenty centimetres (FIRST) survey (Becker et al. 1995), broadly following the techniques described by Best et al. (2005a)

for the earlier SDSS DR2 sample. The parent sample for the DR7 matching is the 927,552 galaxies in the value-added spectroscopic catalogues produced by the group from the Max Planck Institute for Astrophysics, and Johns Hopkins University (hereafter MPA-JHU), and available at <http://www.mpa-garching.mpg.de/SDSS/> (cf. Brinchmann et al. 2004). These galaxies were cross-matched with the NVSS and FIRST radio sources following the method of Best et al. (2005a), but adopting the improvement described by Donoso et al. (2009) for identification of sources without FIRST counterparts. The cross-matching goes down to a flux density level of 5 mJy, which means that the sample probes down to radio luminosities of $L_{1.4\text{GHz}} \approx 10^{23} \text{ W Hz}^{-1}$ at redshift $z = 0.1$. The sample of detected radio sources is presented in Table 1.

The next step was separation of the radio-AGN from star-forming galaxies. This has been improved since the DR2 sample, and now makes use of an optimal combination of three different methods: the method based on 4000Å break strengths and the ratio of radio luminosity to stellar mass, used in Best et al. (2005a); a method based on the ratio of radio to emission line luminosity, similar to that presented in Kauffmann et al. (2008); a standard ‘BPT’ emission-line diagnostic method (Baldwin et al. 1981; Kauffmann et al. 2003a). Appendix A provides full details of the combined method. The resultant classifications are provided in Table 1. The radio luminosity functions for star-forming galaxies and radio-loud AGN separately provide broad confirmation of the success of the classifications (cf. Section 3.1). Further tests have been carried out to ensure that none of the results of this paper is dependent upon the specific details of the SF-AGN separation method.

For the current paper, analysis is restricted to radio sources within the ‘main galaxy sample’ (Strauss et al. 2002), comprising those galaxies with magnitudes in the range $14.5 < r < 17.77$, and further restricted to the redshift range $0.01 < z < 0.3$. Within this sample there are 9,168 radio sources, of which 7,302 are classified as radio-AGN. The median redshift of the radio-AGN is $z = 0.16$, and 1,245 are located at redshift $z \leq 0.1$, to which redshift range some of the analyses are restricted.

Properties of the radio source host galaxies are drawn from the value added catalogues of the MPA-JHU group. In particular, these include total stellar masses (Kauffmann et al. 2003b), accurate emission line fluxes, after subtraction of the modelled stellar continuum to account for underlying stellar absorption features (Tremonti et al. 2004), parameters determined directly from the spectra such as 4000Å break strengths and galaxy velocity dispersions (cf. Brinchmann et al. 2004), and a compendium of basic parameters from the imaging data such as galaxy magnitudes, colours, sizes and structural parameters (see York et al. 2000, for more details). As noted by the MPA-JHU group, the formal line flux uncertainties quoted in the MPA-JHU DR7 catalogue significantly underestimate the true values (as determined by comparing derived line fluxes of sources observed multiple times), and so the line flux uncertainties have been scaled by the factors recommended by the MPA-JHU team.

Table 1. Properties of the 18286 SDSS radio galaxies. Only the first 20 sources are listed here: the full table is available electronically. The first three columns give the identification of the targetted galaxies through their SDSS plate and fibre IDs and the date of the observations. Columns 4 to 6 give the RA, Dec and redshift of the galaxies. Column 7 gives the integrated flux density of the source as measured using the NVSS. Column 8 provides the radio classification of the source, following Best et al (2005): class 1 are single-component NVSS sources with a single FIRST match; class 2 are single-component NVSS sources resolved into multiple components by FIRST; class 3 are single-component NVSS sources without a FIRST counterpart; class 4 sources are those which have multiple NVSS components. Where a galaxy has a central FIRST component, the integrated flux density and offset from the optical galaxy of that central FIRST component are given in columns 9 and 10. Column 11 provides a flag classifying the source as either a radio-loud AGN (1) or a star-forming galaxy (0), according to the criteria described in Appendix A. Column 12 indicates whether the source is included in the full statistical “main sample” studied in this paper (ie. SDSS main sample target with $14/5 \leq r \leq 17.77$). Columns 13 and 14 indicate whether selected radio-loud AGN are classified as LERGs or HERGs, respectively (if such classification is possible; sources with 0 for both cases are unclassifiable using current data).

Plate ID	Julian Date	Fibre ID	RA (J2000) (hr)	Dec (deg)	z	S_{NVSS} 1.4 GHz (Jy)	Radio Class	S_{FIRST} 1.4 GHz (Jy)	Offset (")	AGN	Main Samp	LERG	HERG
266	51602	5	9.784226	-0.81043	0.4486	0.0069	1	0.0042	1.76	1	0	0	0
266	51602	26	9.797071	-0.34230	0.1348	0.0963	1	0.1010	1.26	1	1	1	0
266	51602	100	9.742905	-0.74164	0.2038	0.0068	1	0.0025	0.46	1	1	1	0
266	51602	109	9.782474	-0.25218	0.1304	0.0075	1	0.0043	0.51	1	1	0	0
266	51602	134	9.720425	-0.54706	0.3679	0.0091	2	0.0000		1	0	0	0
266	51602	150	9.758252	-0.36839	0.0530	0.0104	1	0.0010	2.02	0	1	0	0
266	51602	179	9.746165	-0.50828	0.3693	0.0059	1	0.0053	0.16	1	0	0	0
266	51602	235	9.706746	-0.00139	0.1459	0.0054	1	0.0049	0.43	0	1	0	0
266	51602	439	9.720012	0.41417	0.0252	0.0081	3	0.0000		0	0	0	0
266	51602	504	9.764199	0.63871	0.0303	0.0052	1	0.0028	2.09	0	1	0	0
266	51602	507	9.758241	0.25554	0.1291	0.0275	1	0.0269	0.32	1	0	1	0
266	51602	550	9.776251	0.46721	0.4505	0.0088	1	0.0058	0.44	1	0	0	0
266	51602	554	9.787119	0.66564	0.0201	0.0180	1	0.0131	0.79	1	1	1	0
266	51602	559	9.786605	0.70274	0.0305	0.0063	1	0.0045	2.72	0	1	0	0
266	51602	577	9.785432	0.73798	0.2616	0.0489	1	0.0094	0.78	1	1	1	0
266	51602	617	9.805367	0.78802	0.2112	0.0082	1	0.0078	0.66	1	1	0	0
266	51630	361	9.706815	1.14969	0.4498	0.0523	1	0.0454	0.56	1	0	1	0
266	51630	529	9.772283	1.08112	0.5768	0.0146	1	0.0112	0.41	1	0	0	0
267	51608	19	9.907105	-0.92869	0.3583	0.1848	1	0.1839	0.77	1	0	1	0
267	51608	34	9.944658	-0.02334	0.1391	0.1660	4	0.0022	0.27	1	1	1	0
...
...

2.2 High/low excitation classification of the sample

A key requirement of the current analysis is an ability to separate the radio source sample into the two fundamentally-different AGN classes. For consistency with previous works on radio source samples, the nomenclature of “high-excitation” and “low-excitation” radio sources (HERGs and LERGs) will be adopted in this paper to denote these.

The work of Laing et al. (1994), based on very powerful radio-AGN from the 3CR sample, suggested a fairly pronounced division between the two classes. Laing et al. classified as HERGs those sources which had the line flux ratio $[\text{OIII}] 5007 / \text{H}\alpha > 0.2$ and an equivalent width of the $[\text{OIII}]$ line $\text{EW}_{[\text{OIII}]} > 3\text{\AA}$ (where emission line equivalent widths are assigned positive values). Tadhunter et al. (1998) similarly found that low-excitation sources in the 2Jy radio sample, with $\text{EW}_{[\text{OIII}]} < 10\text{\AA}$, stand out from other galaxies in both their $[\text{OIII}] 5007 / [\text{OII}] 3727$ line ratio and the ratio of emission line to radio luminosity. Lower luminosity radio samples, however, show a less-clear division between the two classes, since the emission line luminosities

of the high-excitation sources correlate strongly with radio luminosity (Rawlings & Saunders 1991) and so become much weaker (and less easy to distinguish from LERG lines) in low-luminosity systems (cf. Zirbel & Baum 1995; Kauffmann et al. 2008).

More recent analyses separating HERGs and LERGs have been carried out for large samples of radio galaxies (e.g. Buttiglione et al. 2010; Cid Fernandes et al. 2010; Baldi & Capetti 2010), largely based on emission line diagnostics to separate Seyfert from LINER galaxies devised by Kewley et al. (2006). Note that a growing literature of work (e.g. Cid Fernandes et al. 2011, and references therein) indicates that a significant proportion of LINERs are not due to AGN activity, but rather the emission lines are photo-ionised by post-asymptotic giant branch (post-AGB) stars in old galaxies: such cases can be identified as having an equivalent width of the $\text{H}\alpha$ line below 3\AA (Cid Fernandes et al. 2011). In the radio galaxies studied here, the radio activity confirms that an AGN must be present, but this does not rule out the possibility that the weak emission lines could still have a post-AGB origin.

Buttiglione et al. (2010) have defined an “excitation index” parameter, combining four

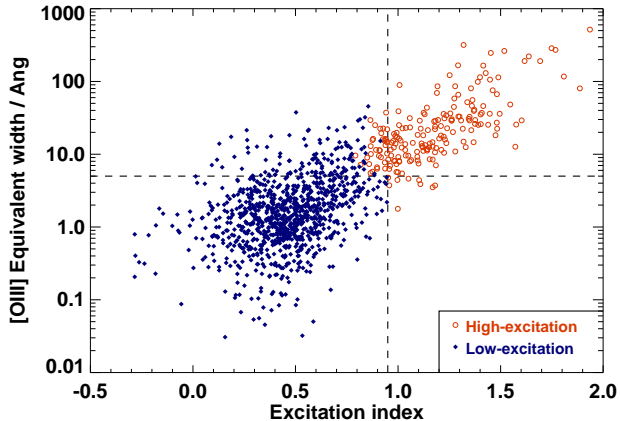


Figure 1. The distribution of the HERG/LERG-classified radio sources on the [OIII] equivalent width versus excitation index (Buttiglione et al. 2010) plane, for galaxies with both parameters measured. This demonstrates the broad consistency of the two main approaches used to classify the radio sources.

emission line ratios: $EI = \log_{10}([\text{OIII}]/\text{H}\beta) - \frac{1}{3} [\log_{10}([\text{NII}]/\text{H}\alpha) + \log_{10}([\text{SII}]/\text{H}\alpha) + \log_{10}([\text{OI}]/\text{H}\alpha)]$.

They demonstrate this parameter to be bimodal and use it to classify the galaxies, dividing the LERG and HERG populations at a value of $EI = 0.95$. For the SDSS radio galaxy sample defined in Section 2.1, in many cases the full set of emission lines needed to classify the host galaxies via the Excitation Index are either not detected, or the signal-to-noise of the detections is low. Therefore a multiple approach was adopted to carry out the classifications, working down the following series of possibilities for each source until a classification was derived.

(i) If all six emission lines were detected and the excitation index was at least 1σ away from 0.95, the radio source was classified using the excitation index [783 LERG; 95 HERG].

(ii) If four lines were reliably detected for one of the individual Kewley et al. (2006) diagnostic diagrams and the source lay at least 1σ from the division line, then that diagnostic diagram was used for classification [330 LERG; 2 HERG].

(iii) If the equivalent width of the [OIII] emission line was at least 1σ above 5\AA then the source was classified as high excitation [65 HERG].

(iv) Classification options (i)–(iii) were repeated but with the 1σ criterion removed [305 LERG; 30 HERG].

(v) If [NII] and $\text{H}\alpha$ emission line measurements were available for the source, then the [NII]/ $\text{H}\alpha$ vs [OIII]/ $\text{H}\alpha$ emission line diagnostic of Cid Fernandes et al. (2010) was used, using either a detection or a limit (if definitive) for the [OIII] emission line [769 LERG; 24 HERG].

To illustrate the consistency of these cuts, Figure 1 shows the distribution of the classified galaxies on the $\text{EW}_{[\text{OIII}]} \text{ vs } EI$ plane, for galaxies with both parameters measured. It is clear that the radio sources do show a good correlation and that both methods can provide suitable classifications. There is a small population of LERGs with relatively high [OIII] equivalent widths but low excitation in-

dices, and therefore a risk that classification method (iii) may lead to contamination of the HERG sample by such sources. However, such contamination is expected to be small: of the 65 sources classified by method (iii), 53 have excitation index measurements within 1σ of 0.95, and all of the remainder have a limiting $[\text{OIII}]/\text{H}\alpha \gtrsim 1$, strongly suggesting they are indeed HERGs.

Despite using all of these different mechanisms, only about a third of the radio sources were able to be classified. Many are simply undetected in emission lines, suggesting that they are likely to be LERGs – although in some cases this may just be due to the relative faintness of the source. To investigate a possible mechanism for classifying these sources, the left panel of Figure 2 shows the distribution of [OIII] line luminosity versus radio luminosity for the classified sources. As discussed above, the two populations do occupy different regions of this plane¹, although there is significant overlap. The solid line in the figure represents an approximate lower limit of the distribution of the HERGs, and so the 3883 sources with emission line luminosities, or limits, below this can therefore be fairly securely classified as LERGs. As demonstrated in the right panel of Figure 2, this allows robust classification of all but four of the $z < 0.1$ subsample of radio galaxies.

3 FUNDAMENTAL PROPERTIES OF THE RADIO SOURCES

3.1 Local radio luminosity functions of HERGs and LERGs

Radio luminosity functions were calculated in the standard way, as $\rho = \sum_i 1/V_i$ (Schmidt 1968; Condon 1989), where V_i is the volume within which source i could be detected. This is calculated as $V_i = V_{\text{max}} - V_{\text{min}}$, where V_{max} and V_{min} are the volumes enclosed within the observed sky area out to the upper and lower redshift limits, respectively, at which each source would be included in the sample. Redshift limits were determined by the joint radio and optical selection criteria, namely a radio cut-off of 5 mJy and optical cut-offs of $14.5 < r < 17.77$, as well as any imposed redshift limit for the analysis (e.g. $0.01 < z < 0.3$). The sky area of the overlapping region between the SDSS DR7 spectroscopic survey and the FIRST radio survey, after removal of noisy regions around very powerful radio sources, was calculated to be 2.17 steradians. The summed radio luminosity function of all radio sources, together with its separation into star-forming galaxies and radio-loud AGN, are provided in Table 2 and shown in Figure 3, and are in excellent agreement with previous determinations (Machalski & Godlowski 2000; Sadler et al. 2002; Best et al. 2005a; Mauch & Sadler 2007). Uncertainties quoted are the statistical Poissonian errors only; at some luminosities these are so small that they will be under-estimates, with systematic errors dominating.

Local radio luminosity functions were derived individually for LERGs and HERGs; these are also tabulated in Table 2 and are shown in Figure 4. In order to minimise the potential influence of unclassified sources (typically found

¹ Radio-quiet quasars would lie above and to the left of the HERG sources (e.g. Xu et al. 1999).

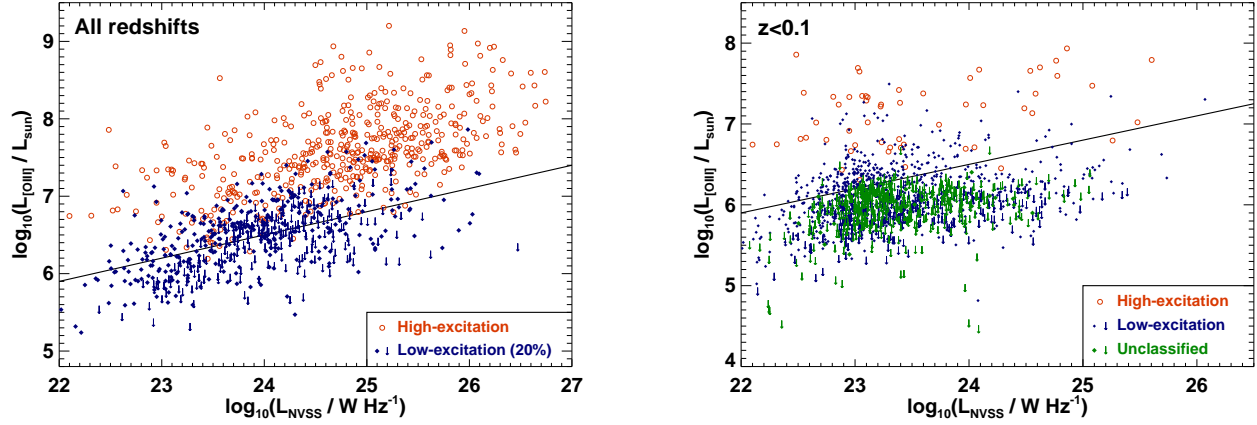


Figure 2. *Left:* the [OIII] emission line luminosity versus radio luminosity for HERG/LERG-classified radio sources. The solid line indicates an approximate lower limit to the distribution of the HERGs, below which unclassified sources can be classified as LERGs with reasonable confidence. Note that only 20% (randomly selected) of LERGs are plotted to avoid over-crowding of the figure. *Right:* the same plot, but only for radio sources with $z < 0.1$, and also including the unclassified galaxies. It can be seen that all but four of the unclassified galaxies in this redshift range can be robustly classified as LERGs using the criterion derived from the left panel.

Table 2. The local radio luminosity functions at 1.4 GHz, derived separately for the HERG and LERG populations. The first column shows the range of 1.4 GHz radio luminosities considered in each bin. The second and third columns show the total number of radio sources and the space density of these, in units of number per $\log_{10}L$ per Mpc^3 , detected out to $z = 0.3$. Columns 4 to 7 show the radio sources split into star-forming galaxies and radio-loud AGN. The eighth column gives the maximum redshift considered for the LERG/HERG analysis, in order to minimise the number of unclassified sources. The numbers and space densities of LERGs, HERGs, and unclassified sources, respectively, are given in columns 9 to 14. Uncertainties are statistical Poissonian uncertainties only. Note that the unclassified sources have negligible contribution compared to the LERG population, but for some bins of luminosity they would make a significant additional contribution if added to the HERG sample (see also Figure 4).

$\log L_{1.4\text{GHz}}$ W Hz^{-1}	All radio sources		Star-forming		Radio-AGN		z_{max}	LERGs		HERGs		Unclassified	
	N	$\log_{10}\rho$	N	$\log_{10}\rho$	N	$\log_{10}\rho$		N	$\log_{10}\rho$	N	$\log_{10}\rho$	N	$\log_{10}\rho$
22.0-22.3	297	$-3.09^{+0.03}_{-0.03}$	284	$-3.11^{+0.03}_{-0.04}$	13	$-4.44^{+0.15}_{-0.23}$	0.10	12	$-4.46^{+0.16}_{-0.25}$	1	$-5.74^{+0.25}$		
22.3-22.6	385	$-3.49^{+0.02}_{-0.03}$	357	$-3.54^{+0.03}_{-0.03}$	28	$-4.45^{+0.05}_{-0.04}$	0.10	24	$-4.51^{+0.05}_{-0.06}$	4	$-5.64^{+0.19}_{-0.33}$		
22.6-22.9	532	$-3.87^{+0.02}_{-0.02}$	388	$-4.00^{+0.02}_{-0.03}$	144	$-4.45^{+0.04}_{-0.04}$	0.10	138	$-4.46^{+0.04}_{-0.05}$	5	$-6.01^{+0.13}_{-0.26}$	1	-6.72
22.9-23.2	674	$-4.22^{+0.02}_{-0.02}$	298	$-4.57^{+0.03}_{-0.03}$	376	$-4.48^{+0.02}_{-0.03}$	0.10	339	$-4.49^{+0.02}_{-0.03}$	9	$-6.09^{+0.13}_{-0.18}$		
23.2-23.5	882	$-4.56^{+0.02}_{-0.02}$	221	$-5.13^{+0.03}_{-0.03}$	661	$-4.69^{+0.02}_{-0.02}$	0.10	248	$-4.73^{+0.03}_{-0.03}$	12	$-6.09^{+0.11}_{-0.15}$	3	-6.66
23.5-23.8	1358	$-4.75^{+0.01}_{-0.01}$	126	$-5.69^{+0.04}_{-0.05}$	1232	$-4.80^{+0.01}_{-0.01}$	0.13	377	$-4.91^{+0.02}_{-0.02}$	12	$-6.42^{+0.11}_{-0.15}$	10	-6.48
23.8-24.1	1615	$-4.90^{+0.02}_{-0.01}$	52	$-6.35^{+0.06}_{-0.08}$	1563	$-4.91^{+0.02}_{-0.02}$	0.15	454	$-4.91^{+0.07}_{-0.09}$	10	$-6.69^{+0.12}_{-0.17}$	8	-6.77
24.1-24.4	1327	$-5.08^{+0.01}_{-0.01}$	19	$-6.83^{+0.11}_{-0.15}$	1308	$-5.09^{+0.01}_{-0.02}$	0.17	427	$-5.19^{+0.02}_{-0.02}$	15	$-6.62^{+0.10}_{-0.14}$	14	-6.70
24.4-24.7	949	$-5.25^{+0.02}_{-0.02}$	3	$-7.43^{+0.23}_{-0.51}$	946	$-5.26^{+0.02}_{-0.02}$	0.17	275	$-5.38^{+0.03}_{-0.03}$	15	$-6.61^{+0.10}_{-0.13}$	1	-7.85
24.7-25.0	561	$-5.54^{+0.02}_{-0.02}$	0	—	561	$-5.54^{+0.02}_{-0.02}$	0.20	228	$-5.66^{+0.03}_{-0.03}$	16	$-6.70^{+0.10}_{-0.13}$		
25.0-25.3	303	$-5.82^{+0.03}_{-0.03}$	0	—	303	$-5.82^{+0.03}_{-0.03}$	0.25	206	$-5.91^{+0.03}_{-0.04}$	21	$-6.76^{+0.09}_{-0.12}$	5	-7.63
25.3-25.6	103	$-6.32^{+0.05}_{-0.06}$	0	—	103	$-6.32^{+0.05}_{-0.06}$	0.25	57	$-6.44^{+0.06}_{-0.07}$	13	$-6.98^{+0.09}_{-0.11}$		
25.6-25.9	47	$-6.58^{+0.07}_{-0.08}$	0	—	47	$-6.58^{+0.07}_{-0.08}$	0.30	29	$-6.82^{+0.08}_{-0.10}$	17	$-6.95^{+0.10}_{-0.14}$	1	-8.55
25.9-26.2	12	$-7.18^{+0.12}_{-0.17}$	0	—	12	$-7.18^{+0.12}_{-0.17}$	0.30	9	$-7.41^{+0.13}_{-0.19}$	3	$-7.64^{+0.17}_{-0.28}$		
26.2-26.5	3	$-7.78^{+0.21}_{-0.43}$	0	—	3	$-7.78^{+0.21}_{-0.43}$	0.30	0	—	3	$-7.78^{+0.21}_{-0.43}$		

at higher redshifts) and yet retain sufficient volume for the rarer luminous sources, the upper limit of the redshift range used to calculate the radio source space density was increased with increasing radio luminosity, as indicated in Table 2. Figure 4 illustrates the maximum effect that the residual unclassified sources could have on the HERG luminosity function, even if all of them were HERGs: although there are small changes to some data points, the overall interpretation and conclusions are unaffected. The potential influence of unclassified sources on the radio luminosity function of the LERGs is completely negligible.

Figure 4 shows that, as expected, LERGs dominate the radio source population at relatively low radio luminosities, while the HERGs begin to dominate at the highest luminosities, beyond $P_{1.4\text{GHz}} \sim 10^{26} \text{W Hz}^{-1}$. However, what is clear (and goes against standard simplifying assumptions in the literature) is that both populations are found across the full range of radio luminosities studied: even at radio luminosities

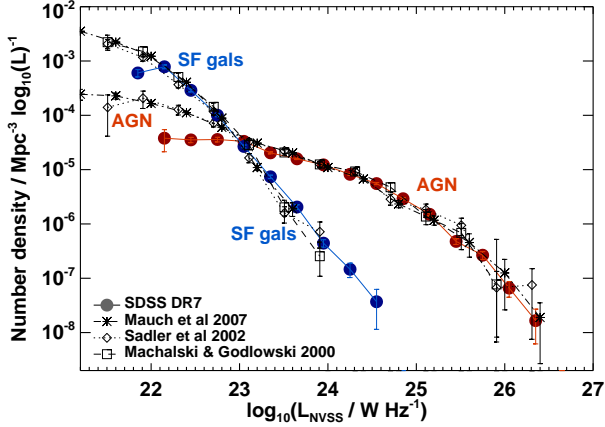


Figure 3. The local radio luminosity function at 1.4 GHz derived separately for radio-loud AGN and star-forming galaxies. Filled points connected by solid lines indicate the data derived in this paper. For comparison, the results of Machalski & Godlowski (2000) using the Las Campanas Redshift Survey, Sadler et al. (2002) using the 2-degree field Galaxy Redshift Survey (2dFGRS), and Mauch et al. (2007) using the 6-degree field Galaxy Survey (6dFGS) are shown.

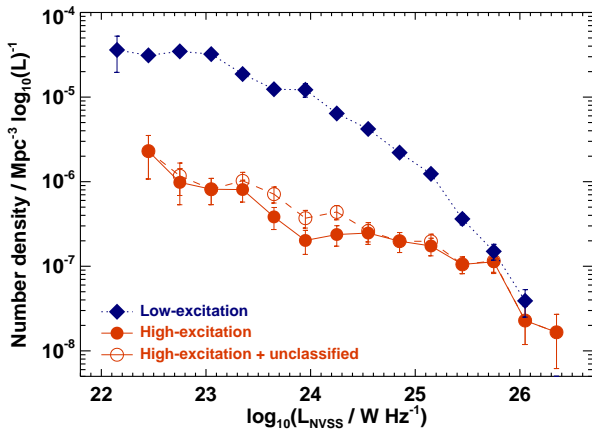


Figure 4. The local radio luminosity function at 1.4 GHz, derived separately for the HERG and LERG populations. Note how both populations are found across the full range of radio luminosities studied.

ties around $P_{1.4\text{GHz}} \sim 10^{23} \text{W Hz}^{-1}$ the HERGs constitute a few percent of the overall radio-loud AGN population².

3.2 The cosmic evolution of HERGs and LERGS

The cosmic evolution of the HERG and LERG populations can be individually investigated by using the V/V_{max} test.

² Note that although there may be some contamination of the low-luminosity HERG population by radio-quiet quasars or Seyfert galaxies, the bulk of these are expected to be genuine radio-loud AGN: as detailed in Appendix A, the separation of star-forming galaxies from AGN was designed to exclude the radio-quiet quasars and Seyfert galaxies from the AGN category.

Taking account of the lower and upper redshift limits (see Section 3.1), the value of $(V - V_{\text{min}})/(V_{\text{max}} - V_{\text{min}})$ was calculated for each source. These were then averaged for HERGs and LERGs separately within radio luminosity bins; once again, to minimise the effect of unclassified sources, a varying upper redshift limit was imposed for the analysis in each radio luminosity bin. The mean values are presented in Table 3 and displayed in Figure 5.

The HERG population displays clear evidence for cosmic evolution at all radio luminosities studied, in the sense of there being a tendency for the sources to be located at larger distances than the median³. In contrast, the LERG population is broadly consistent with a mean $V/V_{\text{max}} \simeq 0.5$ (with the possible exception of the highest radio luminosity bin). The LERGs therefore show little or no evidence for any cosmic evolution. Combined with the results of Section 3.1, this result has important implications for understanding the evolution of the radio luminosity function as a whole, whereby the differential cosmic evolution seen between powerful and less powerful radio sources (Longair 1966) may be driven by the switch in the dominant population with radio luminosity (cf. Figure 4). At high radio luminosities the HERGs dominate and, being a strongly-evolving population, lead to strong evolution of the overall radio source space density at these luminosities (a factor \sim thousand increase in space density out to redshift 2–3; cf. Dunlop & Peacock 1990; Rigby et al. 2011, and references therein). In contrast, at low radio luminosities the LERGs dominate the population, leading to the weak cosmic evolution seen in the low-luminosity radio population (a factor 1.5–2 increase in space density out to $z \sim 0.5$, e.g. Sadler et al. 2007; Donoso et al. 2009). Indeed, even this evolution may be driven to a large extent by the evolution of the HERGs: locally these contribute $\lesssim 10\%$ of the population at low luminosities, but if they increase in space density by an order of magnitude out to $z \approx 0.5$ (as they do at higher radio luminosities) then they would become comparable in numbers to the LERGs and lead to the observed doubling of the overall space density.

3.3 Eddington-scaled accretion rates of HERGs and LERGS

As discussed in the introduction, a popular hypothesis for the difference between LERGs and HERGs relates to the

³ Many HERGs are classical-double radio sources, sometimes with no detected radio core. The possibility exists that sources without cores might be missed by the cross-matching procedure at low redshifts due to the large angular separation of the components. This would mean that z_{min} should be higher than estimated, and could lead to an upward bias in $(V - V_{\text{min}})/(V_{\text{max}} - V_{\text{min}})$. In order to ensure that this is not the origin of the observed evolution of the HERGs, all HERGs with no detected radio core were examined to determine the lowest redshift at which the cross-matching procedure would have included them in the sample, under the worst-case scenario that no additional FIRST components would be detected. For only three sources would this lead to a change in the estimate of z_{min} and these each lead to a change in the relevant $(V - V_{\text{min}})/(V_{\text{max}} - V_{\text{min}})$ value of significantly less than 0.01, which is negligible compared to the associated errors.

Table 3. V/V_{\max} determinations for the LERG and HERG populations separately, in various ranges of radio luminosity. In each luminosity range, an upper redshift limit (z_{\max}) is defined for the analysis (and given in column 2) in order to reduce the number of unclassified sources to negligible levels.

$\log_{10} L_{1.4\text{GHz}}$ W Hz $^{-1}$	z_{\max}	$\langle (V - V_{\min}) / (V_{\max} - V_{\min}) \rangle$	
		LERG	HERG
23.0-23.5	0.13	0.50 ± 0.01	0.54 ± 0.05
23.5-24.0	0.13	0.51 ± 0.01	0.63 ± 0.07
24.0-24.5	0.17	0.52 ± 0.01	0.59 ± 0.06
24.5-25.0	0.20	0.53 ± 0.01	0.55 ± 0.04
25.0-25.5	0.20	0.50 ± 0.02	0.55 ± 0.06
25.5-26.0	0.30	0.52 ± 0.04	0.59 ± 0.05
26.0-26.5	0.30	0.60 ± 0.10	0.83 ± 0.14

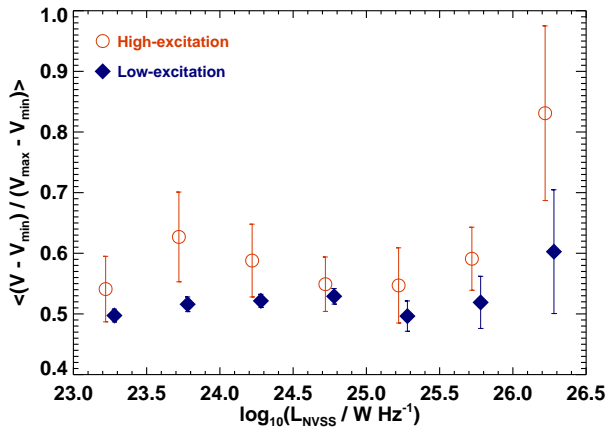


Figure 5. The cosmic evolution, as a function of radio luminosity, of the HERG and LERG populations separately, as demonstrated using the V/V_{\max} test.

Eddington-scaled accretion rates on to the black hole. The Eddington-scaled accretion rate can be estimated for the radio sources by comparing the total energetic output of the black hole, calculated as the sum of the radiative luminosity and the jet mechanical luminosity, with the Eddington luminosity.

The bolometric radiative luminosity of each radio source was estimated from the observed luminosity of the [OIII] 5007 emission line, using the relation determined by Heckman et al. (2004): $L_{\text{rad}} = 3500 L_{\text{OIII}}$. Where the [OIII] line was not detected, an upper limit to the radiative luminosity was set instead. The uncertainty on individual estimates of the bolometric radiative luminosity is ≈ 0.4 dex, from the scatter around the L_{rad} vs L_{OIII} relation (Heckman et al. 2004).

The jet mechanical luminosity was estimated from the 1.4 GHz radio luminosity, using the relation of Cavagnolo et al. (2010), $L_{\text{mech}} = 7.3 \times 10^{36} (L_{1.4\text{GHz}} / 10^{24} \text{W Hz}^{-1})^{0.70} \text{W}$. This relation was determined using the energies associated with cavities evacuated by radio sources in the hot X-ray gas haloes of giant ellipticals, groups and clusters of galaxies. It is in broad agreement with minimum-energy synchrotron

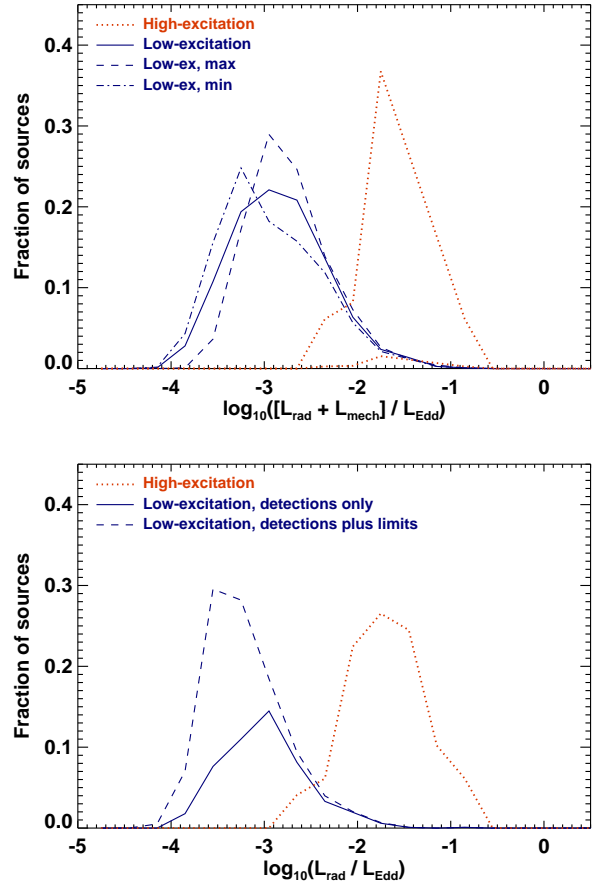


Figure 6. *Top:* The distribution of Eddington-scaled accretion rates for the LERG and HERG populations separately. Analysis is limited to $z < 0.1$, in which redshift range essentially all radio sources could be robustly classified. For the LERGs, the solid line shows the best-estimate distribution, using the calculated values of the radiative luminosity. The dashed line shows the distribution if, for all sources which are undetected in [OIII], the 3σ upper limit to the [OIII] luminosity is used to calculate the radiative luminosity. The dot-dash line shows the distribution if the emission lines of all galaxies with H α equivalent width below 3\AA are assumed not to have an AGN origin. These distributions therefore represent the allowed extremes of the LERG distribution, and show that the result is broadly similar in all three cases. For the HERGs, the dotted line is plotted with two different normalisations: the upper line shows the fraction of sources relative to the total number of HERGs, while the lower line shows the fraction relative to the total number of LERGs to allow direct comparison of numbers with the LERGs. *Bottom:* The distributions are shown considering only the radiative luminosity (ie. ignoring the mechanical energy in the radio jets). For LERGs, the dashed line indicates the maximal distribution calculated using either measurements of, or 3σ upper limit to, the [OIII] luminosity. The solid line indicates the subset of these which are measurements rather than limits.

estimates of Willott et al. (1999). The scatter around the L_{mech} vs $L_{1.4\text{GHz}}$ relation is observed to be about 0.7 dex (Cavagnolo et al. 2010).

The black hole mass of the radio source host galaxy was estimated from the velocity dispersion of the galaxy (σ_*), as measured in the SDSS spectrum, using the

well-established $M_{\text{BH}}-\sigma_*$ relation. The determination of Tremaine et al. (2002) was adopted: $\log(M_{\text{BH}}/M_{\odot}) = 8.13 + 4.02\log(\sigma_*/200\text{km s}^{-1})$. The black hole masses thus derived define the Eddington limit for each radio source, $L_{\text{Edd}} = 1.3 \times 10^{31} M_{\text{BH}}/M_{\odot} \text{W}$. The intrinsic scatter in the $M_{\text{BH}}-\sigma_*$ relation is less than 0.3 dex.

Combining these three relations, the Eddington-scaled accretion rate was derived for each radio source, as $\lambda = (L_{\text{rad}} + L_{\text{mech}})/L_{\text{Edd}}$. In cases where [OIII] was undetected (ie. signal-to-noise below 3) then the radiative luminosity was considered to be negligible compared to the mechanical luminosity, and the Eddington-scaled accretion rate was calculated from the mechanical luminosity alone. For these sources, a maximum value for the Eddington-scaled accretion rate was also calculated based on the upper limit to the [OIII] line luminosity ($\lambda_{\text{max}} = (L_{\text{rad,max}} + L_{\text{mech}})/L_{\text{Edd}}$). For sources where [OIII] was detected, but the equivalent width of the H α emission line was below 3\AA , the possibility was considered that the emission lines arise from photo-ionisation from post-AGB stars, instead of from the AGN (see Section 2.2 and Cid Fernandes et al. 2011). For these sources a minimum value for the Eddington-scaled accretion rate was determined, based only on the mechanical luminosity: $\lambda_{\text{min}} = L_{\text{mech}}/L_{\text{Edd}}$.

The upper panel of Figure 6 shows the distribution of Eddington-scaled accretion rates for the HERG and LERG populations separately; analysis is limited to $z < 0.1$, in which redshift range essentially all radio sources are robustly classified. For the LERGs, distributions are shown for each of λ , λ_{min} and λ_{max} : the three distributions are similar, demonstrating that the high- λ end of the distribution of Eddington-scaled accretion rates for LERGs is robustly described, regardless of the assumptions adopted (it should be noted that the low λ end of the LERG distributions is influenced by the radio selection criteria which will lead to minimum detectable values of L_{mech} : the true distribution may extend to much lower values of λ than indicated by Figure 6). The Eddington-scaled accretion rates of the HERG and LERG populations are clearly fundamentally different: LERGs typically display accretion rates below one per cent of the Eddington rate, whereas HERGs typically accrete at higher Eddington rates (as is also found for radio-quiet AGN in SDSS; cf. Kauffmann & Heckman 2009). This result very strongly implies that Eddington-scaled accretion rate on to the black hole is a primary factor in determining the nature of the accretion flow. The difference in the derived Eddington-scaled accretion rates between HERGs and LERGs is largely driven by the estimate of accretion rates onto the black holes (particularly the difference in L_{rad} , calculated from L_{OIII}) but also in part by HERGs typically being hosted by galaxies with less massive black holes (see Section 4).

For LERGs, the uncertainty in individual λ measurements is ≈ 0.7 dex, dominated by the intrinsic scatter in the L_{mech} vs $L_{1.4\text{GHz}}$ relation. For HERGs, the radiative luminosity is generally much larger than the mechanical luminosity, and so the uncertainty in λ measurements is ≈ 0.4 dex. These large uncertainties will make the observed distributions of accretion rate broader than the intrinsic ones. Therefore, although there is some overlap in the accretion-rate distributions of the LERG and HERG populations, with examples of both classes being found between a few tenths

and a few percent of Eddington, the results would be entirely consistent with a complete dichotomy whereby the LERG/HERG classification is entirely determined by the Eddington-scaled accretion rate (cf. Merloni & Heinz 2008). Alternatively, the overlap in accretion rates between the two classes may imply that, although accretion rate is the primary determinant, other factors may also be important in determining the nature of the accretion flow on to the black hole (black hole spin is an obvious candidate). The current dataset cannot definitively distinguish between these possibilities, because the lack of knowledge of the precise width and shape of the distribution of the uncertainties means that a robust deconvolution of the distributions is not possible. It is worthy of note, however, that if the observed LERG and HERG distributions are simply deconvolved with Gaussians of width 0.7 and 0.4 dex, respectively, then the two deconvolved distributions become entirely distinct, with a clean separation occurring at 1 percent of Eddington.

Finally, the lower panel of Figure 6 shows the distributions considering only the radiative luminosity of the sources ($\lambda_{\text{rad}} = L_{\text{rad}}/L_{\text{Edd}}$), ie. ignoring the mechanical luminosity of the radio jets. This is a somewhat unphysical comparison since it ignores the major energetic output of the LERGs, but is nevertheless included for comparison with other works in the literature which have defined the Eddington ratio in this way. The division between the two populations is even more clear in this analysis.

4 THE NATURE OF THE RADIO SOURCE HOST GALAXIES

Differences in host galaxy properties between the HERG and the LERG populations may provide interesting insight in to either the triggering mechanism of the radio activity, or the effect of the radio source on its host galaxy. Early work with relatively small samples compared radio galaxies with strong emission lines against those with weak or absent lines, and suggested that the strong emission line sources were less luminous, with lower velocity dispersions, bluer colours and lower mass-to-light ratios (ie. younger stellar populations; Smith & Heckman 1989; Smith et al. 1990). These results have been confirmed with much larger radio source samples by Kauffmann et al. (2008), who studied the differences between SDSS-selected radio sources with and without detectable emission lines, and found the host galaxies of emission line radio sources to have lower stellar masses, lower velocity dispersions, lower 4000\AA break strengths, and stronger Balmer absorption features than those without emission lines. However, it is important to note that many LERGs do display emission lines, and so these results should be tested with properly defined LERG and HERG samples.

Lin et al. (2010) also studied large samples of radio galaxies selected from SDSS, in their case separated into different radio morphological types (Fanaroff and Riley Class 1 and 2 sources – FR1/2; Fanaroff & Riley 1974). These two radio morphological classes show a broad overlap with the LERG and HERG classes, respectively, and therefore many differences between LERGs and HERGs may also be reflected by differences between FR1s and FR2s. For this reason, many previous analyses of host

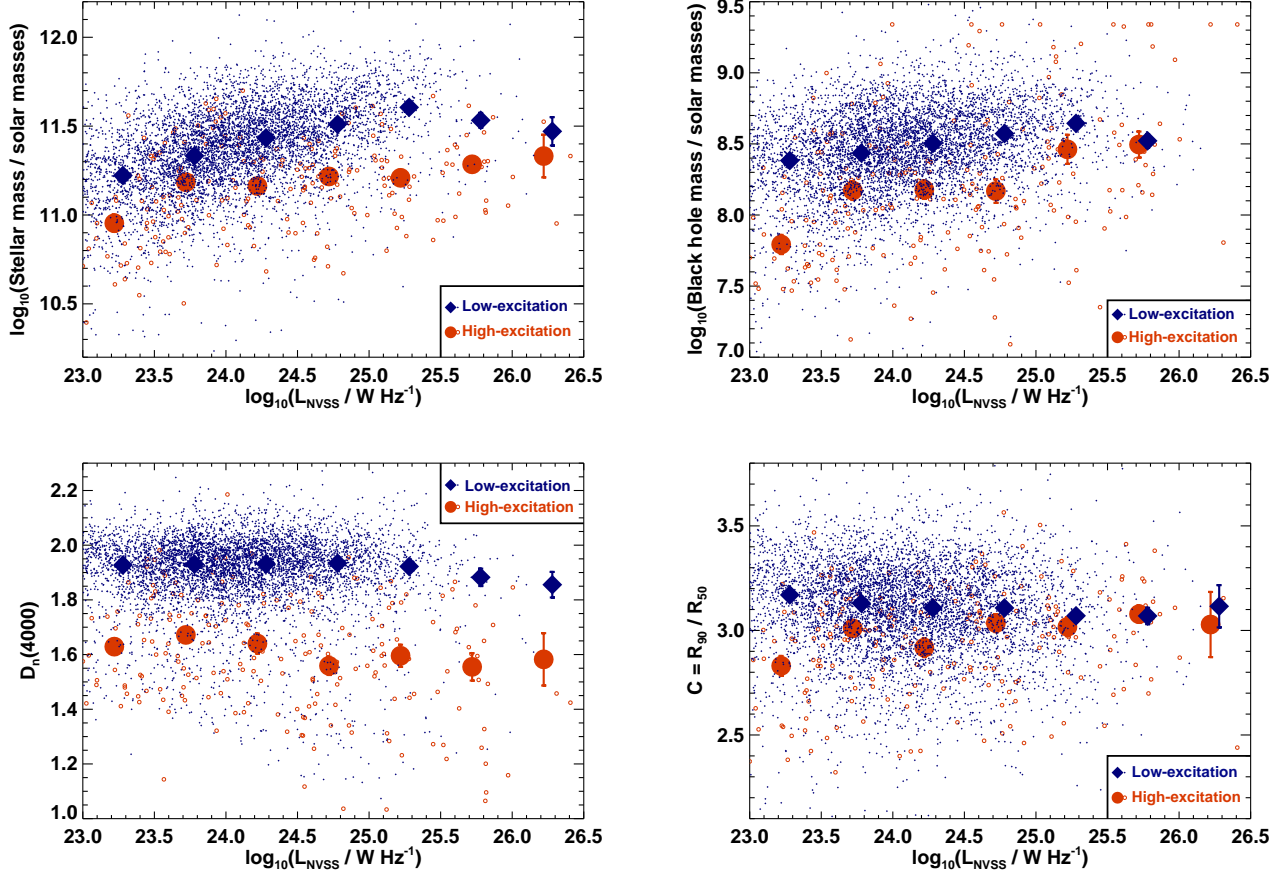


Figure 7. The distributions of stellar mass (upper left), black hole mass (upper right), 4000Å break strength (lower left) and concentration index ($C = R_{90}/R_{50}$, where R_{90} and R_{50} are the radii containing 90% and 50% of the light, respectively; lower right), as a function of radio luminosity, for the LERG and HERG populations separately. The larger symbols indicate the mean values for each population in radio luminosity bins.

galaxy properties, accretion rates, and luminosity functions have concentrated on differences between the FR1/2 classes (e.g. Ledlow & Owen 1996; Ghisellini & Celotti 2001; Cao & Rawlings 2004; Rigby et al. 2008; Gendre et al. 2010, and references therein). However, there are substantial differences between the HERG/LEHG and FR1/2 segregations, since a significant population of LERG FR2s exists (Laing et al. 1994). Indeed, Lin et al. (2010) found the most significant differences when they compared the host galaxy properties of the most edge-brightened FR2s with strong emission lines against those of the other radio sources: this is closer to a HERG/LEHG split. They found this FR2 subset to be hosted by lower mass galaxies, live in sparser environments (cf. Prestage & Peacock 1988; Smith & Heckman 1990), and have higher accretion rates than the rest of the radio source population. Again this argues for the need to investigate clean LERG and HERG samples.

Figure 7 shows the distributions of stellar mass, black hole mass, 4000Å break strength, and concentration index ($C = R_{90}/R_{50}$, where R_{90} and R_{50} are the radii containing 90% and 50% of the light in the r-band) for the host galaxies of the LERG and HERG populations, as a func-

tion of radio luminosity⁴. It is immediately apparent that the HERG selection picks out host galaxies which are less massive and have lower black hole masses than those of the LERGs, in line with the results of Kauffmann et al. (2008) and Lin et al. (2010), and earlier works. The 4000Å breaks strengths of the HERGs are also lower than those of the LERGs at all radio luminosities, indicating younger stellar populations (note that there is no issue of AGN light contamination; see discussion in Kauffmann et al. 2008). At low radio luminosities the concentration indices of the HERGs are also lower.

Many properties of galaxies in the local Universe correlate strongly with the stellar mass. The difference in 4000Å breaks strength between LERGs and HERGs in Figure 7 cannot therefore be properly interpreted until it is known whether it is simply driven by the lower typical stellar mass of the HERGs. To address this, matched samples of LERGs and HERGs were created. For each HERG, a search was made for LERGs which were matched to ± 0.02 in z , ± 0.1 in $\log M$, ± 0.1 in $\log M_{\text{BH}}$ and ± 0.25 in $\log L_{\text{NVSS}}$. If at least

⁴ Note that the same result for concentration index is found if an upper redshift limit of $z = 0.15$ is applied, indicating that any effects of seeing on the measurement of C are unimportant.

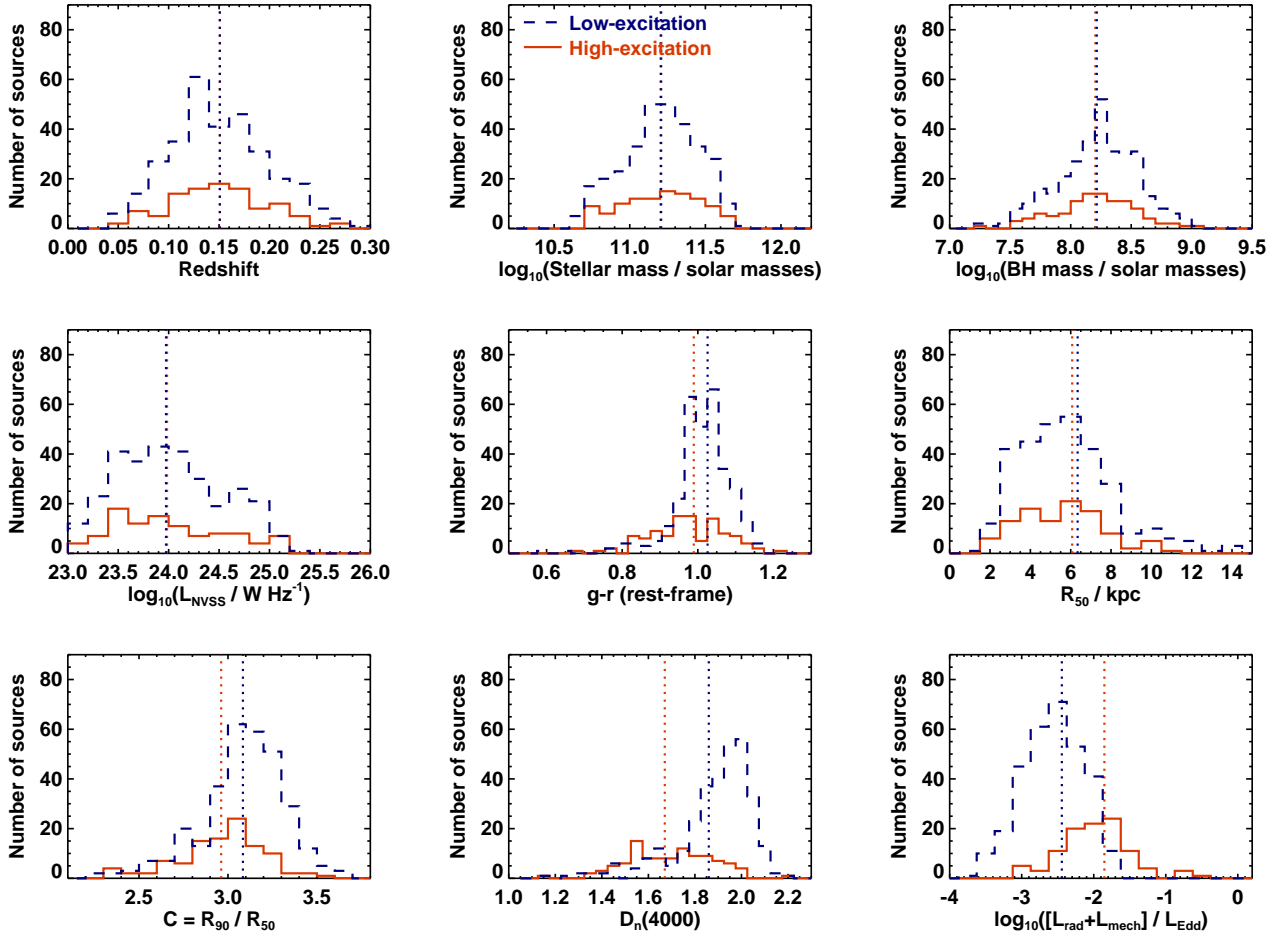


Figure 8. Histograms showing the distribution of radio source and host galaxy properties for samples of LERGs and HERGs which have been matched in redshift, stellar mass, black hole mass, and radio luminosity (with three LERGs matched to each HERG). The first four panels indicate the success of this matching, with the distributions of LERGs and HERGs agreeing well in these four parameters. The remaining panels show differences between the HERG and LERG populations in galaxy colours, sizes, concentration indices, 4000Å break strengths, and Eddington-scaled accretion rates. Vertical dotted lines indicate the mean values for each population.

three such LERGs were found, then three of these were randomly selected for the matched sample. If three matches could not be found then the HERG was excluded from the analysis.

Figure 8 shows histograms of a variety of host galaxy properties for the matched LERG and HERG samples. The first four panels illustrate the distributions of redshift, stellar mass, black hole mass and radio luminosity for the matched samples, and demonstrate the success of the matching. The remaining five panels show the distributions of galaxy colour ($g-r$), size (R_{50} in kpc), concentration index, 4000Å break strength and Eddington-scaled accretion rate for the matched LERGs and HERGs. HERGs are seen to be bluer, smaller, less concentrated, and have lower 4000Å breaks than LERGs of the same stellar and black hole mass and radio luminosity. The offset in galaxy sizes is of marginal significance, as calculated by KS-tests on 1000 iterations of the random matching selection, but the offsets of the other four parameters are each significant at $> 99.9\%$ significance level. The difference in accretion rates is still extremely strong in the matched samples (note that the me-

dian of the LERG distribution is higher than in Figure 6 because the matching with the HERGs pushes the LERG sample towards higher radio luminosities and lower black hole masses). The bluer colours and lower 4000Å breaks are consistent with the HERGs being associated with ongoing star formation activity, as is also seen in similar radio-quiet AGN (e.g. Kauffmann et al. 2003a). The smaller average sizes and lower concentration indices may be related to the triggering mechanism of the sources. In particular, if LERGs are often fuelled by accretion from their hot gas haloes, then they might be more preferentially located at the centres of groups or clusters (cf. Kauffmann et al. 2008; Lin et al. 2010), where host galaxies are typically larger and may have more extended (cD-type) light profiles.

5 SUMMARY AND INTERPRETATION

A large sample of radio sources drawn from the SDSS has been classified into high- and low-excitation radio galaxies, and the nature of these two different populations has been investigated. The main results are:

- Local radio luminosity functions have been derived separately for the LERGs and HERGs for the first time. Both populations are found across the full range of radio luminosities studied, although LERGs dominate the population at low radio luminosities and HERGs at high luminosities. The two populations appear to be switching in dominance at $L_{1.4\text{GHz}} \sim 10^{26} \text{ W Hz}^{-1}$.

- HERGs show evidence for strong cosmic evolution at all radio luminosities, while LERGs are consistent with little or no evolution. This difference, coupled with the changing population mix as a function of radio luminosity, helps to drive the strong luminosity-dependence of the evolution seen in the overall radio luminosity function.

- The accretion rates of the HERGs and LERGs are fundamentally different. HERGs typically have accretion rates between one and ten percent of Eddington. LERGs, in contrast, predominantly accrete at rates of below one percent of Eddington.

- HERGs are hosted by galaxies of lower mass and lower black hole mass than LERGs of the same radio luminosity. The host galaxies of HERGs are also bluer and have lower 4000Å break strengths than LERGs of the same mass and radio luminosity, indicating the presence of associated star formation. LERGs are larger and have more extended light profiles than HERGs, consistent with the interpretation that they are more likely to be hosted by central galaxies of groups and clusters.

These results are consistent with the developing picture of radio-loud AGN, in which HERGs are fuelled at relatively high rates in radiatively-efficient standard accretion disks by cold gas, perhaps brought in through mergers and interactions, and with some of the cold gas leading to associated star formation. The requirement for significant cold gas supplies means that these sources are much more prevalent at earlier cosmic epochs where merger rates and gas fractions were larger. In contrast, LERGs are fuelled at relative low rates, through radiatively-inefficient accretion flows, largely by gas associated with the hot X-ray haloes surrounding the galaxy or its group or cluster (although gas from any other source fuelling the black hole at low accretion rates would also lead to a LERG). Regardless of whether the accretion occurs directly from the hot gas through the Bondi mechanism, or after the hot gas has cooled, this gas source allows the setting up of an AGN feedback cycle, since this is the gas directly affected by any radio-AGN activity (cf. Best et al. 2006). In this picture, LERGs will be associated with massive galaxies, which have old passive stellar populations. Given that massive galaxies show little evolution out to $z \sim 1$, the lack of cosmic evolution seen in the LERG population is as expected.

One of the most interesting results coming out of this study is the almost distinct nature of the accretion rate properties of the LERG and HERG classes. This is in line with earlier indications comparing FR1 and FR2 sources (Ghisellini & Celotti 2001), and with more recent results for a switch in accretion rate between BL Lacs and flat-spectrum radio quasars (Wu et al. 2011; Ghisellini et al. 2011). This result fits in well with theoretical calculations of accretion modes onto black holes (Narayan & Yi 1995), and is in line with what is found in galactic X-ray binary systems. X-ray binaries display three well-defined spectral

states (e.g. Fender et al. 2004, and references therein): a ‘low/hard’ state in which the source is characterised by hard X-ray emission, low-power radio jets are ubiquitous, and the radio and X-ray luminosities are correlated (Gallo et al. 2003, possible analogue to the radiatively inefficient AGN state); a ‘high/soft’ state dominated by a thermal X-ray component characteristic of a standard thin accretion disk (possible analogue to radio-quiet quasar-like AGN); a short-lived ‘intermediate’ or ‘transition’ state between the two, where both the thermal accretion disk and powerful radio jets are seen (possible analogue to radio-loud quasar-like AGN). The switch between these different accretion states in X-ray binary systems has been shown to depend upon the accretion rate onto the black hole, with the switch occurring at between 1 and a few percent of the Eddington rate (Maccarone 2003) - very similar to the value derived in this paper for radio-AGN.

Körding et al. (2006) demonstrated that spectral states analogous to those of X-ray binaries could be identified in local AGN, while other analogies between the black holes in X-ray binaries and those in AGN have been uncovered through examinations of the relationships between radio and X-ray luminosities and black hole mass (the so-called ‘Fundamental plane of black hole activity’; Merloni et al. 2003; Falcke et al. 2004). On the basis on those results, and the assumption that not only do AGN show these same three spectral states but that there is also the same dependence on accretion rate between them, synthesis models of AGN have been constructed (e.g. Merloni & Heinz 2008). The results in this paper offer strong evidence in support of these AGN synthesis models, and the broad principles of the analogy of AGN with X-ray binary systems, by both confirming previous indications of a lower limit to the accretion rate of radiatively efficient AGN, and demonstrating that an upper limit of around a percent Eddington applies to the radiatively-inefficient population.

ACKNOWLEDGEMENTS

PNB is grateful for financial support from the Leverhulme Trust. The research makes use of the SDSS Archive, funding for the creation and distribution of which was provided by the Alfred P. Sloan Foundation, the Participating Institutions, the National Aeronautics and Space Administration, the National Science Foundation, the U.S. Department of Energy, the Japanese Monbukagakusho, and the Max Planck Society. The research uses the NVSS and FIRST radio surveys, carried out using the National Radio Astronomy Observatory Very Large Array: NRAO is operated by Associated Universities Inc., under co-operative agreement with the National Science Foundation. The authors would like to thank Guinevere Kauffmann, Andrea Merloni and Martin Hardcastle, amongst others, for interesting discussions on this topic, and an anonymous referee for helpful suggestions.

REFERENCES

Abazajian K. et al. 2009, *ApJ Supp.*, 182, 543

- Allen S. W., Dunn R. J. H., Fabian A. C., Taylor G. B., Reynolds C. S., 2006, *MNRAS*, 372, 21
- Antonucci R., 1993, *ARA&A*, 31, 473
- Birzan L., Rafferty D. A., McNamara B. R., Wise M. W., Nulsen P. E. J., 2004, *ApJ*, 607, 800
- Baldi R. D., Capetti A., 2010, *A&A*, 519, 48
- Baldwin J. A., Phillips M. M., Terlevich R., 1981, *PASP*, 93, 5
- Becker R. H., White R. L., Helfand D. J., 1995, *ApJ*, 450, 559
- Best P. N., Kaiser C. R., Heckman T. M., Kauffmann G., 2006, *MNRAS*, 368, L67
- Best P. N., Kauffmann G., Heckman T. M., Brinchmann J., Charlot S., Ivezić Ž, White S. D. M., 2005b, *MNRAS*, 362, 25
- Best P. N., Kauffmann G., Heckman T. M., Ivezić Ž, 2005a, *MNRAS*, 362, 9
- Best P. N., Röttgering H. J. A., Longair M. S., 2000, *MNRAS*, 23, 311
- Best P. N., von der Linden A., Kauffmann G., Heckman T. M., Kaiser C. R., 2007, *MNRAS*, 379, 894
- Böhringer H., Voges W., Fabian A. C., Edge A. C., Neumann D. M., 1993, *MNRAS*, 264, L25
- Bower R. G., Benson A. J., Malbon R., Helly J. C., Frenk C. S., Baugh C. M., Cole S., Lacey C. G., 2006, *MNRAS*, 370, 645
- Brinchmann J., Charlot S., Heckman T., Kauffmann G., Tremonti C., White S. D. M., 2004, *astro-ph/0406220*
- Burns J. O., 1990, *AJ*, 99, 14
- Buttiglione S., Capetti A., Celotti A., Axon D. J., Chibera M., Macchetto F. D., Sparks W. B., 2010, *A&A*, 509, 6
- Cao X., Rawlings S., 2004, *MNRAS*, 349, 1419
- Carilli C. L., Perley R. A., Harris D. E., 1994, *MNRAS*, 270, 173
- Cattaneo A., Best P. N., 2009, *MNRAS*, 395, 518
- Cattaneo A. et al. 2009, *Nat*, 460, 213
- Cavagnolo K. W., McNamara B. R., Nulsen P. E. J., Carilli C. L., Jones C., Birzan L., 2010, *ApJ*, 720, 1066
- Cid Fernandes R., Stasińska G., Mateus A., Vale Asari N., 2011, *MNRAS*, 413, 1687
- Cid Fernandes R., Stasińska G., Schlickmann M. S., Mateus A., Vale Asari N., Schoenell W., Sodré L., 2010, *MNRAS*, 403, 1036
- Condon J. J., 1989, *ApJ*, 338, 13
- Condon J. J., Cotton W. D., Greisen E. W., Yin Q. F., Perley R. A., Taylor G. B., Broderick J. J., 1998, *AJ*, 115, 1693
- Croton D. et al. 2006, *MNRAS*, 365, 11
- Donoso E., Best P. N., Kauffmann G., 2009, *MNRAS*, 392, 617
- Dunlop J. S., Peacock J., 1990, *MNRAS*, 247, 19
- Elvis M. et al. 1994, *ApJ Supp.*, 95, 1
- Fabian A. C., 1999, *MNRAS*, 308, L39
- Fabian A. C., Sanders J. S., Taylor G. B., Allen S. W., Crawford C. S., Johnstone R. M., Iwasawa K., 2006, *MNRAS*, 366, 417
- Falcke H., Körding E., Markoff S., 2004, *A&A*, 414, 895
- Fanaroff B. L., Riley J. M., 1974, *MNRAS*, 167, 31P
- Fender R. P., Belloni T. M., Gallo E., 2004, *MNRAS*, 355, 1105
- Ferrarese L., Merritt D., 2000, *ApJ*, 539, L9
- Gallo E., Fender R. P., Pooley G. G., 2003, *MNRAS*, 344, 60
- Gebhardt K. et al. 2000, *ApJ*, 539, L13
- Gendre M. A., Best P. N., Wall J. V., 2010, *MNRAS*, 404, 1719
- Ghisellini G., Celotti A., 2001, *A&A*, 379, L1
- Ghisellini G., Tavecchio F., Foschini L., Ghirlanda G., 2011, *MNRAS*, 414, 2674
- Häring N., Rix H.-W., 2004, *ApJ*, 604, L89
- Hardcastle M. J., Evans D. A., Croston J. H., 2007, *MNRAS*, 376, 1849
- Hart Q. N., Stocke J. T., Hallman E. J., 2009, *ApJ*, 705, 854
- Heckman T. M., Kauffmann G., Brinchmann J., Charlot S., Tremonti C., White S. D., 2004, *ApJ*, 613, 109
- Hine R. G., Longair M. S., 1979, *MNRAS*, 188, 111
- Kauffmann G., Heckman T. M., 2009, *MNRAS*, 397, 135
- Kauffmann G., Heckman T. M., Best P. N., 2008, *MNRAS*, 384, 953
- Kauffmann G. et al. 2003a, *MNRAS*, 346, 1055
- Kauffmann G. et al. 2003b, *MNRAS*, 341, 33
- Kewley L. J., Groves B., Kauffmann G., Heckman T., 2006, *MNRAS*, 372, 961
- King A., 2003, *ApJ*, 596, L27
- Kollmeier J. A. et al. 2006, *ApJ*, 648, 128
- Körding E. G., Jester S., Fender R., 2006, *MNRAS*, 372, 1366
- Laing R. A., Jenkins C. R., Wall J. V., Unger S. W., 1994, in Bicknell G. V., Dopita M. A., Quinn P. J., eds, *The first Stromlo symposium: Physics of active galaxies* Cambridge University Press, Cambridge, p. 201
- Ledlow M. J., Owen F. N., 1996, *AJ*, 112, 9
- Lin Y.-T., Shue Y., Strauss M. A., Richards G. T., Lunnan R., 2010, *ApJ*, 723, 1119
- Longair M. S., 1966, *MNRAS*, 133, 421
- Maccarone T. J., 2003, *A&A*, 409, 697
- Machalski J., Godłowski W., 2000, *A&A*, 360, 463
- McNamara B. R., Rohanizadegan M., Nulsen P. E. J., 2011, *ApJ*, 727, 39
- Magorrian J., Tremaine S., Richstone D., Bender R., Bower G., Dressler A., Faber S., Gebhardt K., Green R., Grillmair C., Kormendy J., Lauer T., 1998, *AJ*, 115, 2285
- Marconi A., Hunt L. K., 2003, *ApJ*, 589, L21
- Martínez-Sansigre A., Rawlings S., 2011, *MNRAS*, p. 543
- Mauch T., Sadler E. M., 2007, *MNRAS*, 375, 931
- McNamara B. R., Nulsen P. E. J., 2007, *ARA&A*, 45, 117
- McNamara B. R. et al. 2000, *ApJ*, 534, L135
- Merloni A., Heinz S., 2007, *MNRAS*, 381, 589
- Merloni A., Heinz S., 2008, *MNRAS*, 388, 1011
- Merloni A., Heinz S., di Matteo T., 2003, *MNRAS*, 345, 1057
- Narayan R., Yi I., 1995, *ApJ*, 452, 710
- Nesvadba N. P. H., Lehnert M. D., De Breuck C., Gilbert A. M., van Breugel W., 2008, *A&A*, 491, 407
- Prestage R. M., Peacock J. A., 1988, *MNRAS*, 230, 131
- Rawlings S., Saunders R., 1991, *Nat*, 349, 138
- Rigby E. E., Best P. N., Brookes M. H., Peacock J. A., Dunlop J. S., Röttgering H. J. A., Wall J. V., Ker L., 2011, *MNRAS*, in press; arXiv:1104.5020
- Rigby E. E., Best P. N., Snellen I. A. G., 2008, *MNRAS*, 385, 310

- Robertson B., Hernquist L., Cox T. J., Di Matteo T., Hopkins P. F., Martini P., Springel V., 2006, *ApJ*, 641, 90
 Sadler E. et al. 2002, *MNRAS*, 329, 227
 Sadler E. et al. 2007, *MNRAS*, 381, 211
 Schmidt M., 1968, *ApJ*, 151, 393
 Shakura N. I., Sunyaev R. A., 1973, *A&A*, 24, 337
 Silk J., Rees M. J., 1998, *A&A*, 331, L1
 Smith E. P., Heckman T. M., 1989, *ApJ*, 341, 658
 Smith E. P., Heckman T. M., 1990, *ApJ*, 348, 38
 Smith E. P., Heckman T. M., Illingworth G. D., 1990, *ApJ*, 356, 399
 Strauss M. A. et al. 2002, *AJ*, 124, 1810
 Tadhunter C. N., Morganti R., Robinson A., Dickson R. D., Villar-Martín M., Fosbury R. A. E., 1998, *MNRAS*, 298, 1035
 Tadhunter C. N. et al. 2011, *MNRAS*, 412, 960
 Tremaine S. et al. 2002, *ApJ*, 574, 740
 Tremonti C. A., Heckman T. M., Kauffmann G., Brinchmann J., Charlot S., White S. D. M., Seibert M., Peng E. W., Schlegel D. J., Uomoto A., Fukugita M., Brinkmann J., 2004, *ApJ*, 613, 898
 Trump J. R. et al. 2009a, *ApJ*, 700, 49
 Trump J. R. et al. 2009b, *ApJ*, 706, 797
 Trump J. R. et al. 2011, *ApJ*, 733, 60
 Wild V., Heckman T., Charlot S., 2010, *MNRAS*, 405, 933
 Willott C. J., Rawlings S., m. Blundell K., Lacy M., 1999, *MNRAS*, 309, 1017
 Wu Q., Xu Y.-D., Cao X., 2011, *Jour. of Astrophys. and Astro.*, 32, 223
 Xu C., Livio M., Baum S., 1999, *AJ*, 118, 1169
 York D. G. et al. 2000, *AJ*, 120, 1579
 Zirbel E. L., Baum S. A., 1995, *ApJ*, 448, 521

APPENDIX A: SEPARATION OF STAR-FORMING GALAXIES AND RADIO-LOUD AGN

This appendix provides details of the techniques used to classify the selected SDSS radio sources as either star-forming galaxies or radio-loud AGN. It is important to clarify that the attempt made here is to classify the origin of the radio emission, and hence that radio-quiet AGN are classified together with the star-forming galaxies, rather than contaminating the radio-loud AGN category.

Three mechanisms for separating the two classes of sources are considered: (i) using the relationship between the 4000Å break strength and the ratio of radio luminosity per stellar mass (cf. Best et al. 2005a), hereafter referred to as the ‘D₄₀₀₀ vs L_{rad}/M’ method; (ii) using emission line diagnostics, in particular the ratio of [OIII] 5007 and Hβ line fluxes, and that of [NII] 6584 and Hα (cf. Baldwin et al. 1981), hereafter referred to as the ‘BPT’ method; (iii) using the relation between the Hα emission line luminosity and the radio luminosity – the ‘L_{Hα} vs L_{rad}’ method. The precise divisions adopted for each of these three methods are described in Section A1 and are illustrated in Figure A1. Following this, the manner in which the results of these methods are combined to produce an overall classification is explained in Section A2.

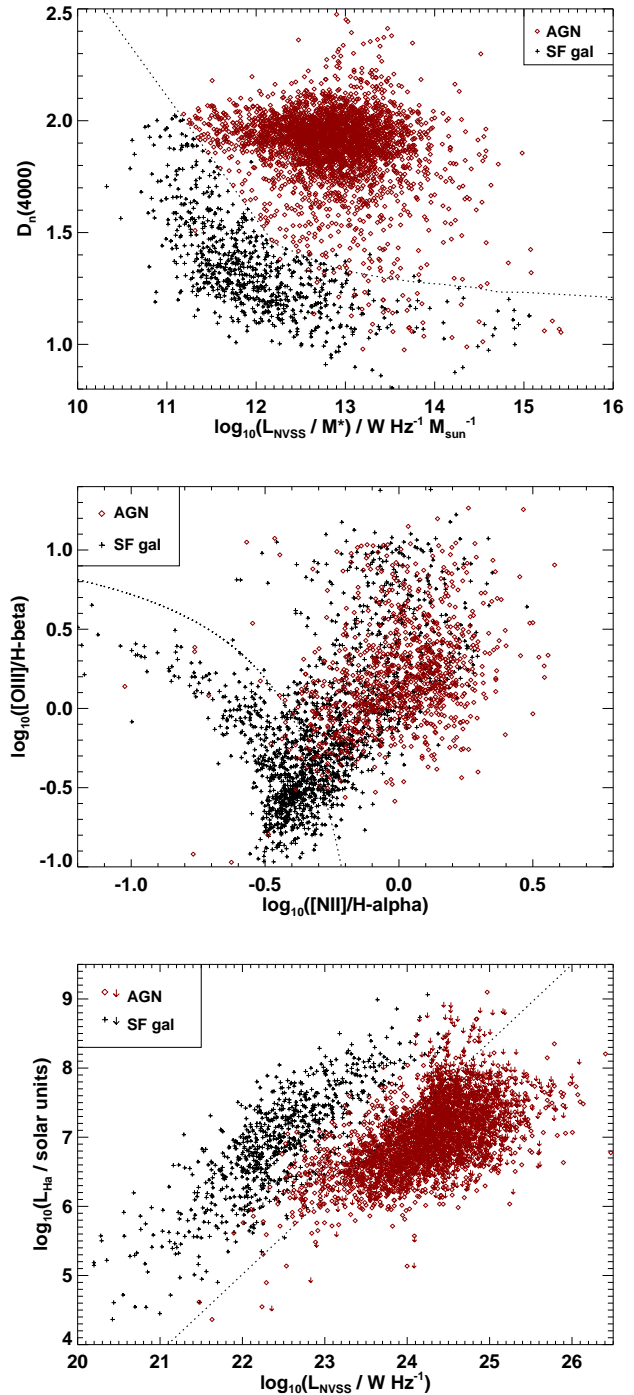


Figure A1. The location of radio sources on the three classification lines used to separate radio-loud AGN from galaxies where the radio emission is powered by star-formation. The top plot is the ‘D₄₀₀₀ vs L_{rad}/M’ method, developed by Best et al. (2005a). The middle plot shows the widely-used ‘BPT’ emission line ratio diagnostic. The lower plot shows the relationship between Hα and radio luminosity. In all plots, the dotted lines indicate the division used for that classification method. Sources plotted as red diamonds are classified as radio-loud AGN in the overall classification, while star-forming galaxies appear as black crosses. In the lower plot, arrows indicate upper limits to the Hα luminosity.

Table A1. The table presents the numbers of sources in each combination of classifications by the three different classification methods, together with the overall classification adopted and the rationale for that classification. It should be emphasised that ‘AGN’ in the classification refers to sources classified as radio-loud AGN, whereas ‘SF’ refers to sources where the radio emission is powered by star-formation (albeit that a radio-quiet AGN may also be present).

D_{4000} vs L_{rad}/M	BPT	$L_{H\alpha}$ vs L_{rad}	No of Sources	Overall class	Rationale for overall classification
AGN	AGN	AGN	1078	AGN	Unambiguous AGN
AGN	AGN	??	0	–	No sources
AGN	AGN	SF	847	AGN	Mostly close to cut line in $L_{H\alpha}$ but clear AGN in other plots
AGN	??	AGN	8053	AGN	All weak-lined, reliable AGN
AGN	??	??	1938	AGN	Weak-lined AGN. Majority high- z . $L_{H\alpha}$ limit nearly allows AGN classification
AGN	??	SF	222	AGN	Clear AGN in D_{4000} . Close to $L_{H\alpha}$ cut; offset from bulk of SF population
AGN	SF	AGN	25	AGN	Radio excess. Near BPT cut line. Probably radio-loud AGN with associated SF
AGN	SF	??	0	–	No sources
AGN	SF	SF	40	SF	Close to D_{4000} cut line. Most have high extinction.
??	AGN	AGN	42	AGN	Clear AGN; almost all have high L_{rad} and high D_{4000} but no mass estimate.
??	AGN	??	0	–	No sources
??	AGN	SF	55	SF	Most likely scenario is radio-quiet AGN with associated SF
??	??	AGN	1166	AGN	Mostly $z > 0.3$. Almost all have high L_{rad} and high D_{4000} but no mass estimate.
??	??	??	1767	AGN	All but six have $z > 0.3$ and $L_{\text{rad}} > 10^{25} \text{WHz}^{-1}$
??	??	SF	12	SF*	Properties mostly appear like SF galaxies; see footnote
??	SF	AGN	0	–	No sources
??	SF	??	0	–	No sources
??	SF	SF	29	SF*	Consistent classification, but see footnote
SF	AGN	AGN	37	AGN	Mostly high z , high L_{rad} . Probably radio-loud AGN with SF activity
SF	AGN	??	0	–	No sources
SF	AGN	SF	1582	SF*	Mostly low luminosity; almost certainly radio-quiet AGN
SF	??	AGN	73	AGN	Mostly high z , high L_{rad} . Probably radio-loud AGN with SF activity
SF	??	??	42	SF*	Clear SF in D_{4000} but too distant for emission line classifications
SF	??	SF	35	SF	Consistent classification
SF	SF	AGN	19	SF*	Mostly low L_{rad} SF galaxies near $L_{H\alpha}$ cut line, but see footnote.
SF	SF	??	0	–	No sources
SF	SF	SF	1224	SF	Unambiguous SF

* In these classes, there exist small populations of objects with $L_{\text{rad}} > 10^{24.5} \text{WHz}^{-1}$ and $z > 0.3$. The properties of these subsets of high L_{rad} , high- z galaxies appear much more like radio-loud AGN. Therefore, although the bulk of these objects are classified overall as SF galaxies, the subsets of $L_{\text{rad}} > 10^{24.5} \text{WHz}^{-1}$ and $z > 0.3$ sources are classified as radio-loud AGN.

A1 The three classification methods

The ‘ D_{4000} vs L_{rad}/M ’ method was developed by Best et al. (2005a), on the basis that star-forming galaxies with a wide range of star formation histories occupy a similar locus in this plane. This is because, for star-forming galaxies, both L_{rad}/M and D_{4000} depend broadly on the specific star formation rate of the galaxy. Radio-loud AGN will have enhanced values of L_{rad} and are thus separable on this plane. Best et al. (2005a) adopted a division line of 0.225 higher in D_{4000} than the track produced by a galaxy with an exponentially declining star formation rate of 3 Gyr e-folding time. They demonstrated that this method was generally very successful by comparison with other methods used in the literature. Further work by Kauffmann et al. (2008) indicated that this selection line may be somewhat too shallow at low values of L_{rad}/M , misclassifying some star-forming galaxies as AGN. Taking account of this, the division line of Best et al. (2005a) was modified such that for $L_{\text{rad}}/M < 12.2$, a straight-line cut is adopted with equation $D_{4000} = 1.45 - 0.55(L_{\text{rad}}/M - 12.2)$. Most radio sources are classifiable by this method, but $\approx 17\%$ of sources are not, due to the lack of a mass estimate in the MPA-JHU SDSS value-added catalogues. These unclassifiable sources are almost always the highest redshift sources, $z > 0.3$, se-

lected in samples other than the ‘main galaxy sample’ (ie. with $r > 17.77$), although small numbers of lower redshift sources where the automated algorithm had failed are also present.

The ‘BPT’ method has been widely used by a number of authors to divide star-forming galaxies from AGN, since the different spectrum of the ionising radiation leads to different emission line ratios. As outlined by Best et al. (2005a), however, there are problems relating to its direct use for identification of a clean radio-loud AGN sample. In particular, it is well-established that AGN and star-formation activity are closely related (e.g. Kauffmann et al. 2003a). Radio-quiet AGN may therefore be detected in the radio on the basis of their on-going star-formation activity and identified as AGN on the basis of their emission line ratios, thus contaminating the radio-loud sample. Nevertheless, the emission line ratios can offer useful information in many cases. Here, the division proposed by Kauffmann et al. (2003a) is adopted, namely that galaxies with $\log([\text{OIII}]/\text{H}\beta) > 1.3 + 0.61 / (\log([\text{NII}]/\text{H}\alpha) - 0.05)$ are classified as AGN. Just under 30% of the radio source sample are classifiable by this method, but the rest lack detections (or definitive limits) for at least one line.

The ‘ $L_{H\alpha}$ vs L_{rad} ’ method is based on the premise that, for star-forming galaxies, both the $H\alpha$ luminosity and the

radio luminosity provide a direct measure of the star formation rate and these properties are therefore correlated. For radio-loud AGN, a far higher radio luminosity to $H\alpha$ luminosity ratio is observed, and so the location of galaxies in the $L_{H\alpha}$ vs L_{rad} plane can be used to identify radio-loud AGN (cf. Kauffmann et al. 2008). Ideally the extinction-corrected $H\alpha$ luminosity would be used, since dust attenuation can decrease the $H\alpha$ -to-radio luminosity ratio of star-forming galaxies. However, this is only possible for the subset of galaxies for which $H\beta$ is also detected, to allow a dust attenuation estimate from the Balmer decrement, and even then the attenuation correction that should be used is different for star-forming galaxies and AGN. Here the observed $H\alpha$ luminosity is therefore used instead, with an adopted division line of $\log(L_{H\alpha}/L_{\odot}) = 1.12 \times (\log(L_{\text{rad}}/\text{WHz}^{-1}) - 17.5)$. This cut is designed to be conservative, in the sense that galaxies classified as radio-loud AGN by this cut should be secure AGN, whereas the SF class may be contaminated by some AGN close to the cut line. Almost 80% of the radio sources are classifiable by this method, either using the observed $H\alpha$ luminosity, or because the upper limit on that luminosity allowed clear classification.

A2 Combination into a final classification

For each of the three classification methods, every radio source is classified as a radio-loud AGN, classified as having its radio emission associated with star formation, or is unclassified. There are therefore 27 possible combinations of classification. Table A1 indicates the number of galaxies in each of these 27 different classes and the resulting classification adopted. These overall classifications are arrived at by examining in detail the properties of the galaxies in each class, especially where different classification methods disagree. For example, in most cases where objects miss the D_{4000} vs L_{rad}/M classification due to the lack of a stellar mass estimate, the values of D_{4000} and L_{rad} are both so high that the galaxy will be classified as an AGN for any plausible value of the stellar mass and so that classification can be securely adopted. Similarly, in some classes with disputed classifications, if the sources lie very clearly within the AGN regime in two of the plots but just on the SF side of the cut line in the third, then that adds weight to an overall AGN classification. The rationale for the final classification is included in Table A1.

Figure 3 shows the radio luminosity functions derived for star-forming galaxies and radio-loud AGN. The smooth nature of the derived luminosity functions, especially at low and high luminosities where small numbers of misclassifications would have pronounced effects, offers broad support to the success of the classification scheme, as does the comparison with previous determinations from Machalski & Godlowski (2000), Sadler et al. (2002) and Mauch & Sadler (2007). The slight offset of the AGN line from previous determinations below a radio luminosity of $L \approx 10^{23} \text{WHz}^{-1}$ may be caused by the different classification of radio-quiet AGN, which here are classified along with the star-forming galaxies. In any case, objects of these low luminosities are excluded from most of the analyses in this paper.